High-Steepness and Low-Loss SAW Filters With Fractional Bandwidth From 3.7% to 12.4% on a Monolithic X-Cut $LiNbO_3/SiO_2/SiC$ Substrate

Xiaoli Fang, *Student Member, IEEE*, Jinbo Wu, *Member, IEEE*, Shibin Zhang, *Member, IEEE*, Pengcheng Zheng, *Graduate Student Member, IEEE*, Juxing He, *Student Member, IEEE*, Xinjian Ke, *Student Member, IEEE*, Kai Huang, Jicong Zhao, *Member, IEEE*, Haiyan Sun, Min Zhou, Xiaomeng Zhao, and Xin Ou, *Senior Member, IEEE*

***Abstract*— To integrate the ladder-type surface acoustic wave (SAW) filters of different frequency bands on a monolithic substrate and improve skirt steepness, a new approach of selectively adjusting the electromechanical coupling coefficient (k_t^2) of built-in resonators without reducing their Q values is investigated. Based on the X-cut $LiNbO_3/SiO_2/SiC$ (LNOSiC) substrate, the in-plane orientations (θ) of the SAW resonators are adjusted to obtain the desired k_t^2, while long dummy electrodes are applied to suppress the transverse leakage of the acoustic field to maintain a high Q value. For resonators with in-plane orientations (θ) from 0° to 42°, the range of k_t^2 is continuously adjustable from 31% to 5%, while the measured maximum *Bode-Q* values are maintained around 1800. By presetting the in-plane orientations of resonators, the n25, n66, n40, 2.4 GHz Wi-Fi, n41, and n78 filters with FBW from 3.7% to 12.4% and out-of-band rejection over 35 dB were demonstrated. On the other hand, to meet the high requirements of steep skirts, the k_t^2 of specific resonators in n41 and 2.4 GHz Wi-Fi filters are selectively reduced. Among a set of n41 filters of different designs, the one with steeper skirts has a shunt resonator with an in-plane orientation of 39° and a corresponding k_t^2 of 7.5%. While the rest of the resonators have a uniform in-plane orientation of 27° with k_t^2 of 18%. The filter demonstrates a 3-dB passband from 2496 to 2685 MHz, a minimal insertion loss (IL) of 1.29 dB, and reaches 16 dB rejection at 2483 MHz, which is the edge of the 2.4 GHz Wi-Fi band. The fabricated 2.4 GHz Wi-Fi filter demonstrates a 3-dB passband of 2388–2482 MHz, a minimum IL of 1.32 dB, and achieves 30 dB rejection at 2496 MHz on the edge of the n41.**

***Index Terms*— Bandwidth, electromechanical coupling coefficient, in-plane orientation, ladder-type filter, monolithic substrate, Q value, skirts steepness, surface acoustic wave (SAW).**

Manuscript received 10 March 2024; revised 3 May 2024; accepted 14 May 2024. This work was supported in part by the National Natural Science Foundation of China under Grant 62293521, Grant 62293524, Grant 62204252, and Grant 62231023; in part by the Young Elite Scientists Sponsorship Program by CAST under Grant 2022QNRC001; in part by the Youth Innovation Promotion Association CAS; and in part by the Shanghai Rising-Star Program under Grant 23QB1405300. *(Xiaoli Fang and Jinbo Wu contributed equally to this work.) (Corresponding authors: Shibin Zhang; Xin Ou.)*

Xiaoli Fang, Jinbo Wu, Pengcheng Zheng, Juxing He, Xinjian Ke, and Xin Ou are with State Key Laboratory of Materials for Integrated Circuits, Shanghai Institute of Microsystem and Information Technology, Chinese Academy of Sciences, Shanghai 200050, China, and also with the Center of Materials Science and Optoelectronics Engineering, University of Chinese Academy of Sciences, Beijing 100049, China (e-mail: ouxin@mail.sim.ac.cn).

Shibin Zhang, Kai Huang, Min Zhou, and Xiaomeng Zhao are with the State Key Laboratory of Materials for Integrated Circuits, Shanghai Institute of Microsystem and Information Technology, Chinese Academy of Sciences, Shanghai 200050, China (e-mail: sbzhang@mail.sim.ac.cn).

Jicong Zhao and Haiyan Sun are with the School of Microelectronics and the School of Integrated Circuits, Nantong University, Nantong 226000, China.

Color versions of one or more figures in this article are available at https://doi.org/10.1109/TMTT.2024.3403916.

Digital Object Identifier 10.1109/TMTT.2024.3403916

I. Introduction

ACOUSTIC filters are widely used in the radio frequency (RF) front end for frequency selection and interference suppression. With the rapid development of wireless communication, the Internet of Things (IoT), and so on, the number of frequency bands in RF front-end modules for mobile communication systems is increasing. In the 5G era, Sub-4 GHz is characterized by multiple bands with varying bandwidths and very narrow gaps between the operating frequency bands. Especially, the frequency gap between the n41 spectrum (2496–2690 MHz) and the 2.4 GHz Wi-Fi spectrum (2400–2483 MHz) is only 13 MHz. Thanks to the superb advantages of miniature size, low cost, lithography-defined frequency, and steady performance, surface acoustic wave (SAW) devices dominate the sub-3.5 GHz RF filter market [1], [2], [3], [4], [5], [6], [7]. For applications within the increasingly crowded frequency bands of mobile communication systems, advanced SAW filters must not only feature steep skirts with low loss in the passband and the rejection in the adjacent bands, but also maintain wideband rejection [8], [9].

Acoustic filters consist of acoustic resonators cascaded in a certain topology. Ladder-type filter topology is widely applied due to its simple structure, low in-band loss, and good out-of-band rejection [9], [10]. The common understanding of ladder filters suggests that a certain minimum electromechanical coupling coefficient (k_t^2) for resonators is necessary to meet the bandwidth and return-loss specifications for a given band [10], [11], [12]. The k_t^2 of resonators is greatly determined by the piezoelectric material platform. The bandwidth of sub-4 GHz frequency bands varies widely, from 0.4% (n71) to 14% (n78). Accordingly, filters for these bands are based on multiple material platforms with different specifications, such as SiO_2/Cu/128° YX $LiNbO_3$ (LN) [13], SiO_2/Cu/42° YX $LiTaO_3$ (LT) [14], 50° YX LT/SiO_2/Si [4], X-cut LN/SiC [12],

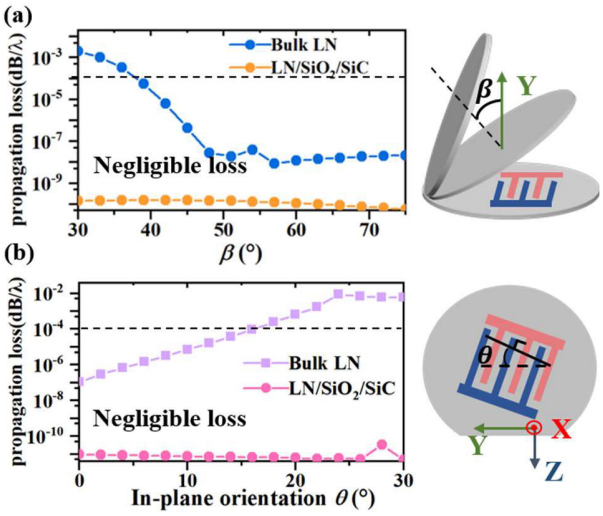

Fig. 1. Simulated propagation loss at the resonance frequency as a function of the Euler angle (a) β in (0°, β°, 0°) LN and (b) θ in (θ°, 90°, 90°).

32° YX LN/SiO_2/poly-Si/Si [15], AlScN FBAR substrate [16]. If multiple band filters can be fabricated on a single piezoelectric material platform, the number of piezoelectric material platforms will be significantly reduced, along with the cost of the RF front end.

Furthermore, to improve filter skirt steepness, early designs are based on intrinsic low k_t^2 resonators. The drawback of this technique is that the coupling capabilities of all the resonators are degraded, leading to poor out-of-band rejection [17], [18]. Additionally, external electrical elements are needed to meet the bandwidth requirement sometimes. In some cases, reducing k_t^2 on only a subset of resonators in the ladder structure will be more advantageous. Because it allows the skirt steepness of the filter to be improved substantially with minimized compromise on other feature parameters [17]. This method of increasing skirt steepness raises the question of how to adjust the k_t^2 of certain resonators in a ladder filter without affecting other properties of those resonators (e.g., Q value).

In recent years, SAW devices based on thin piezoelectric plates [e.g., $LiTaO_3$ (LT) or $LiNbO_3$ (LN)] bonded on heterogeneous substrates have made many exciting breakthroughs, attracting great research interest as an alternative to bulk crystal substrates [2], [7], [15], [19], [20], [21], [22], [23], [24], [25]. Due to the waveguide effects, SAW devices based on piezoelectric heterogeneous substrates break the limitation of conventional bulk materials, on which devices can only achieve low losses in specific cut angles and in-plane orientation [14], [26]. Among them, SH-SAW devices based on the LN/SiO_2/high-velocity substrate (e.g., SiC or Si) material platform have achieved remarkable performance such as large k_t^2, low loss, and controllable temperature coefficients of frequency (TCF) [15], [22], [23], [24], [25], [27], [28]. Compared with the bulk acoustic wave (BAW) filter, SAW filters are more competitive in concurrently addressing various bands, as they capitalize on nothing but tuning interdigital transducers (IDTs) period to define the frequency [12]. Achieving flexible tunability of k_t^2 of SAW resonators is the remaining bottleneck for realizing the monolithic integration of multiband filters and improving skirts steepness. However, current methods of adjusting the k_t^2 require integration with external electrical elements (such as capacitive or inductive), which results in enlarged losses as well as footprints [29], [30].

In this work, based on the X-cut $LiNbO_3$/SiO_2/SiC (LNOSiC) substrate, a new approach to tune the k_t^2 of built-in resonators in filters by adjusting their in-plane orientations is investigated. The electrode structure is optimized to adjust the k_t^2 without increasing loss. By presetting the in-plane orientations of resonators to obtain the desired k_t^2, low-loss filters for multiple frequency bands, including n25, n66, n40, 2.4 GHz Wi-Fi, n41, and n78 have been demonstrated. The fabricated filters exhibit FBW from 3.7% to 12.4% and out-of-band rejection over 35 dB. Furthermore, by selectively reducing the k_t^2 of specific resonators in ladder-type filters, a set of n41 filters are designed, fabricated, and compared. The optimized n41 filter shows an improved skirt steepness and achieves coexistence with the 2.4 GHz Wi-Fi filter.

II. Fundamental Design and Analysis

A. Selection of Piezoelectric Heterogeneous Substrate

Meeting the bandwidth and skirt steepness requirements of filters with different frequency bands on a single piezoelectric material platform raises a problem. The problem is how to adjust the k_t^2 of resonators in a ladder filter without affecting other properties of these resonators. As the in-plane anisotropy of piezoelectric material, the k_t^2 of resonators can be adjusted by simply altering their in-plane orientations [12]. First, the finite element simulation is conducted using periodic 3-D models to calculate the propagating loss of acoustic waves. The simulated attenuations at the resonant frequency of two SAW structures are presented in Fig. 1. The LN thickness and electrode period of both structures are set to 330 nm and 1.6 μm, respectively. The thickness of the SiO_2 layer is set to 500 nm. The estimated losses are only associated with the leakage into the substrate, and other loss mechanisms (electrode resistance, transverse leakage, etc.) are ignored [31]. In the case of normal SAW on bulk LN substrate, the attenuation changes dramatically with the variation of the LN cut angle and in-plane orientation, with low losses being achieved only in a specific range. For the case of the LNOSiC piezoelectric heterogeneous substrate, the attenuation maintains lower than 1×10^{-9} dB/λ. This indicates that for the SH-SAW resonator based on the $LiNbO_3$/SiO_2/high-velocity substrate, acoustic leakage is negligible in any in-plane orientation and cut angle. These results demonstrate that the SH-SAW devices based on the LN heterostructure have the potential to adjust their k_t^2 by altering their in-plane orientation without increasing the loss.

Our previous work has reported high-performance SH-SAW resonators and filters based on the X-cut LN/SiC substrate [6], [20]. However, the resonators based on this substrate can only achieve Rayleigh-SAW suppression under specific in-plane orientations. Deviation from this direction results in an apparent Rayleigh-SAW response between resonant frequency and anti-resonant frequency of SH-SAW [see Fig. 2(b)], which affects the passband performance of the filter. In contrast, the introduction of the 500 nm SiO_2 layer can shift the

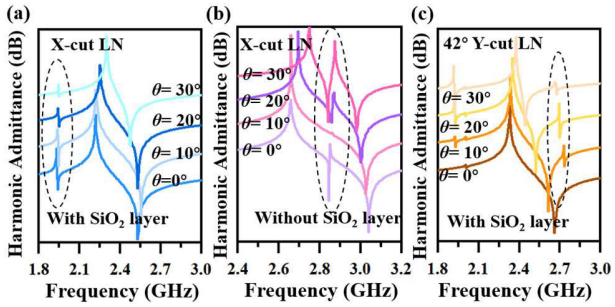

Fig. 2. Simulated harmonic admittance curves of SH-SAW with different in-plane orientations on (a) 330 nm X-cut LN/SiO_2/SiC, (b) 330 nm X-cut LN/SiC, and (c) 330 nm 42° cut Y-LN/SiO_2/SiC substrate.

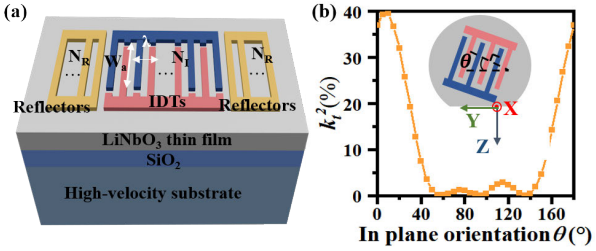

Fig. 3. (a) Schematic of an SH-SAW resonator using the thin-film LN/SiO_2/substrate structure. (b) Simulated k_t^2 based on X-cut LN/SiO_2/SiC substrate with different in-plane orientations.

Rayleigh-SAW response below the resonant frequency of SH-SAW and a significant reduction in the magnitude of the Rayleigh-SAW response can be achieved [see Fig. 2(a)]. Y-cut X propagation LN thin films have also been extensively studied. SH-SAW splitting can be observed in the resonators based on Y-cut LN thin film. This can be interpreted by the presence of piezoelectric coefficient e_{36} [see Fig. 2(c)] when the propagating direction changes. Therefore, X-cut LN/SiO_2/high-velocity substrate-based resonators are preferable for coupling coefficient adjustment via altering the in-plane orientation.

B. Method to Adjust k_t^2 of Resonator

The schematic of a one-port SH-SAW resonator based on an X-cut LN/SiO_2/high-velocity substrate structure is shown in Fig. 3(a). The resonator consists of IDTs on top of the LN thin film, solidly mounted on the SiO_2 and high-velocity substrate. Two grating reflectors are placed at both ends of IDTs. The in-plane anisotropy of the SH-SAW is analyzed under periodic grating using the periodic model. Fig. 3(b) presents the simulated k_t^2 with varying in-plane orientation based on X-cut LNOSiC substrate. The thickness of the $LiNbO_3$, SiO_2, and Al electrodes layer is set to 330, 500, and 130 nm, respectively, and the λ is set to 1.6 μm. Benefitted from the strong in-plane anisotropy of LN, the k_t^2 can be tuned from 0 to nearly 40% by altering in-plane orientation. This offers substantial design freedom, facilitating monolithic integration of filters with different bandwidths. At the same time, it permits the design of ladder filters with steeper passband edge by reducing k_t^2 only on a subset of resonators in the ladder.

In conventional filter design, the most common method of adjusting the k_t^2 of resonators includes placing capacitive or inductive components in series or parallel with the resonator [17], [32]. Fig. 4 demonstrates several methods to adjust the k_t^2 of a resonator, as discussed previously. Our proposed method is to alter the in-plane orientation, which is very simple and prevents the problem of the increased volume and enhanced losses of the filter due to the addition of external electrical components [29], [30].

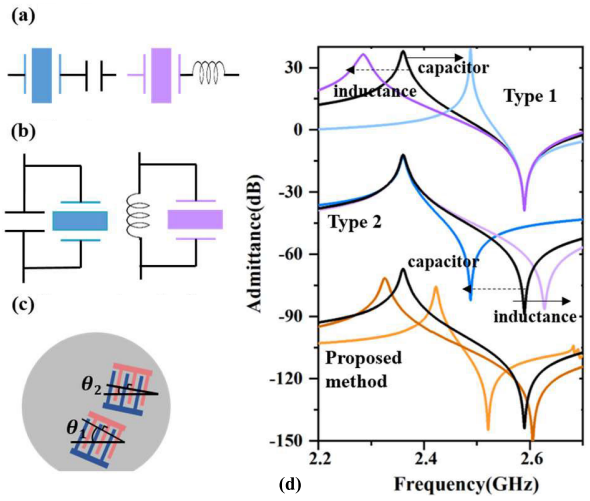

Fig. 4. Methods to adjust k_t^2 of a resonator (a) attach a parallel capacitance (or inductance), (b) attach a series capacitance (or inductance), (c) alter in-plane orientation, and (d) simulated admittance response using different methods.

C. Relationship Between Filter Bandwidth and the k_t^2 of Resonators

Fig. 5(a) depicts the topology of a ladder filter. As shown in Fig. 5(b), in the case of a conventional ladder-type filter, a shunt resonator places a transmission zero (TZ) below the passband with its resonant frequency (f_r), while placing its anti-resonant frequency (f_p) near the center frequency of the passband (f_c). A series resonator places a TZ at the high-frequency side of the passband by its f_p with its f_r in the passband. This concept is commonly exploited and has been covered from a synthesis perspective [33], [34]. Fig. 6 presents the responses of the filters with different bandwidths and their component resonators. The results suggest that the adjustment of filter bandwidth can be achieved by modifying k_t^2 of the built-in resonators. This is achieved with uniform low-pass prototype filter responses maintained (out-of-band rejection, normalized TZs position).

D. Relationship Between Filter Steepness and k_t^2 of the Resonators

As is shown in Fig. 5(b), the steepness of the filter has a large relationship with the position of the TZ. If the TZ is closer to the passband, the passband edge becomes steeper. Therefore, the steepness of the lower passband edge of the filter is sensitive to the k_t^2 of the shunt resonators, while the steepness of the higher passband edge of the filter is sensitive to that of the series resonators. Fig. 7(a) displays the simulated S-parameter responses of three filters with the same passband based on the topology shown in Fig. 5(a). In the case of Filter1,

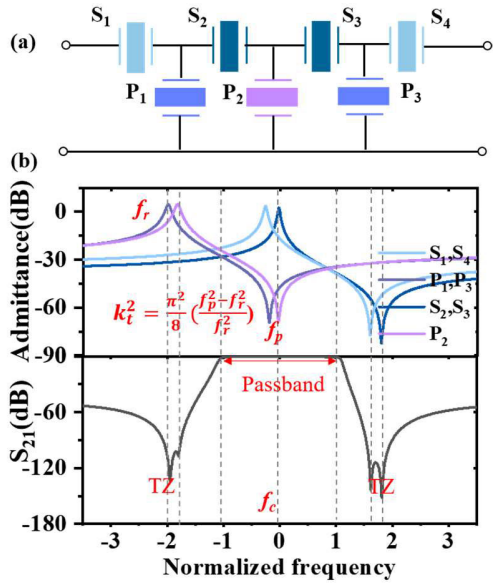

Fig. 5. (a) Topology of a ladder-type filter and (b) transmission response of a filter with its corresponding resonator admittance responses.

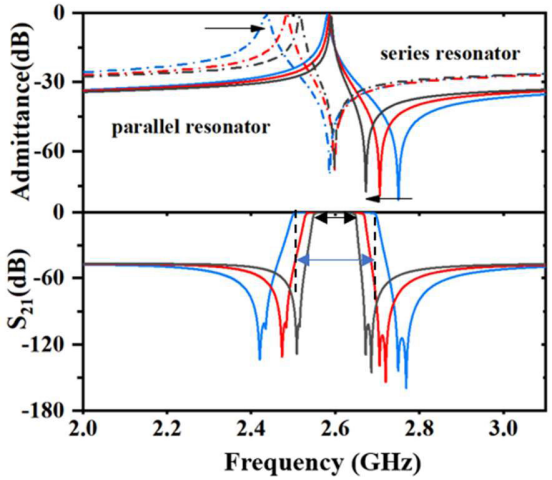

Fig. 6. Simulated transmission response of filters with different bandwidths based on the topology shown in Fig. 5(a), and the admittance response of their corresponding partial resonators.

the k_t^2 of all resonators is 18%; Filter2 employs a simultaneous reduction of all resonators to 16%, resulting in a slight improvement in steepness. Further reduction of the k_t^2 would improve the skirt steepness. However, additional electrical elements would be needed to meet the bandwidth requirement and would further worsen the out-of-band rejection [17]. For Filter 3, the results demonstrate that solely reducing the k_t^2 of the shunt resonator P_2 leads to a much higher steepness on the left side of the passband. The out-of-band rejection of both Filter2 and Filter3 decreases due to the reduction in k_t^2 of the built-in resonators, indicating a tradeoff between skirt steepness and out-of-band rejection. From the simulation results, it is evident that selectively decreasing k_t^2 of the certain resonators in ladder topology yields significant advantages. Because it allows the skirt steepness of a filter to be improved substantially while the impact on other feature parameters is minimized.

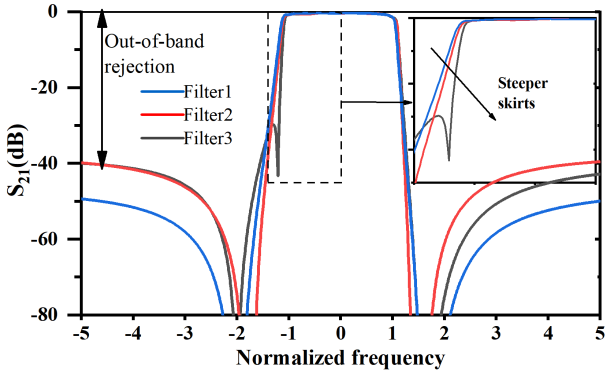

Fig. 7. Simulated and zoomed-in view transmission response of three filters with the same passband based on the topology shown in Fig. 5(a). (The k_t^2 of all resonators in Filter1 is 18%, in Filter2 is16%, and in Filter3 is 18%, except for P_2 which is 7%.)

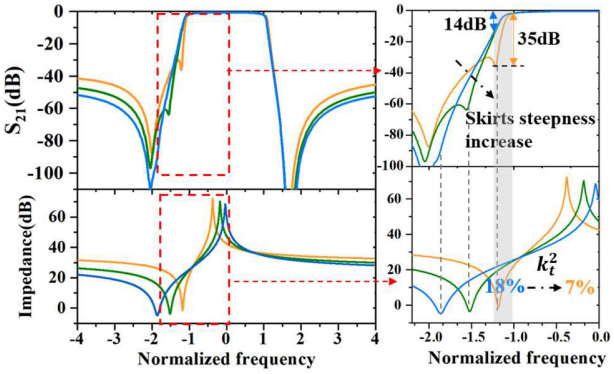

Fig. 8. Simulated transmission responses of filters vary with changes in the k_t^2 of the shunt resonator P_2.

The effect of selectively decreasing the k_t^2 of a specific resonator (P_2) in the filter on the filter skirt steepness is demonstrated in Fig. 8. This indicates that the smaller k_t^2 of the shunt resonator, the steeper the low-frequency skirt steepness of the filter. At the normalized frequency of -1.2, the k_t^2 of resonator P_2 is 18% and the rejection is 14 dB, further reducing k_t^2 to 7% dramatically increases the rejection to 35 dB. Since the k_t^2 of built-in resonators can be adjusted flexibly by altering their in-plane orientations and the skirts steepness of the filter can be altered flexibly.

III. Measured Results of Resonators

The 6-in single-crystalline X-cut $LiNbO_3$ thin film is transferred onto the SiO_2/SiC substrate by an ion-slicing process. Fig. 9(a) shows the photograph of the fabricated 6-in X-cut LN/SiO_2/SiC wafer. The thickness of the $LiNbO_3$ thin film is around 330 $\pm$ 20 nm, and the thickness of SiO_2 is 500 nm. Three groups of SH-SAW resonators with different in-plane orientations are fabricated through electron-beam lithography, metal evaporation, and lift-off process. The metal consists of Ti/Al/Ti with a thickness of 2, 120, and 2 nm, respectively. The optical microscope image of a fabricated resonator is shown in Fig. 9(b), while the corresponding top scanning electron microscope image is shown in Fig. 9(c). The period of the IDTs (λ) is 1.6 μm, the aperture is 20λ, and the number of IDT finger pairs is 100. Tilted IDTs are used to suppress the

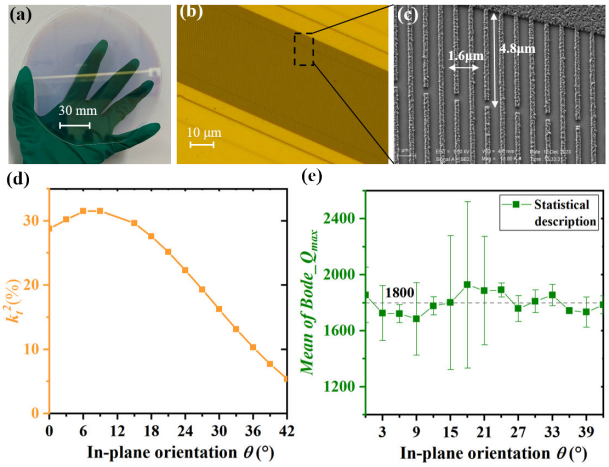

Fig. 9. (a) Optical microscope image of the fabricated 6-in X-cut LN/SiO_2/SiC wafer. (b) Optical microscope image of the fabricated resonator. (c) Top scanning electron microscope image of the fabricated resonator. (d) Measured k_t^2 of resonators with different in-plane orientations. (e) Measured mean *Bode-*$Q_{\max}$ of resonators with different in-plane orientations.

transverse spurious modes, and long dummy electrodes are applied to reduce lateral energy leakage [35], [36], [37], [38].

The frequency responses of the fabricated SAW resonators are characterized using a vector network analyzer (Keysight E5071C) with a terminal impedance of 50 Ω at room temperature in air. Fig. 9(d) summarizes the changes of k_t^2 at various in-plane orientations. The maximum k_t^2 of 31% is reached at the in-plane orientation of 9°, which can be reduced to about 1/6 of that value, i.e., 5.3%, by adjusting the in-plane orientation to 42°. Fig. 10(a) presents a schematic of the IDT structure of the fabricated resonators. The change in the in-plane orientation of the resonator is achieved by rotating the IDT by different angles (θ). The tilted angles (t) of the IDT of resonators with varying in-plane orientations are optimized to suppress the transverse modes. Additionally, the long dummy electrodes are implemented to address the issue of lateral leakage. When θ is 9°, a tilt angle of 20° can ensure a spurious-free response and maintain a high Q value [see Fig. 10(b)]. The k_t^2 of the resonators decreases to 18% when the in-plane orientation is 27° [see Fig. 10(c)]. When the in-plane orientation reaches 33°, the k_t^2 of the resonator decreases to 13%, which is equivalent to the level of conventional LT-based resonators. In the meantime, a Q value comparable to that of LT/SiO_2/Si-based resonators is achieved [39] [see Fig. 10(d)]. Fig. 9(e) presents a summary of the measured average maximum *Bode-Q* (*Bode-*$Q_{\max}$) values of three sets of resonators. Despite some fluctuations in the *Bode-*$Q_{\max}$ due to experimental errors, the measured maximum *Bode-*$Q_{\max}$ values of the resonators are still maintained at around 1800. These experimental results demonstrate that the k_t^2 of the chosen structure can be tuned by altering the in-plane orientation without increasing loss.

IV. Analyses and Measured Results of Filters

A. Multiband Integration

According to the above systematic research, resonators implemented on X-cut LNOSiC structure showcase superior performance in achieving k_t^2 flexible modulation, along with an on-chip wide frequency lithographic tunability, eight ladder-type filters with bandwidth ranging from 3.7 (n25) to 14% (n78) are designed. Table I shows the key design parameters of resonators in the eight SH-SAW filters respectively. The one of series resonators with the smallest capacitance in the filter is divided into two cascaded resonators to improve power durability. On the surface of X-cut LN thin films, the resonators in n66 filters are oriented at a θ of 37.5° to the Y-axis, while in the n25 filters are oriented at a θ of 39°. For the n40 and Wi-Fi filters, the θ of resonators is 36°, while the resonators in the n41 filter have an in-plane orientation of 27°. Due to the large bandwidth of n78, the resonators in this filter are set in the direction with the largest k_t^2.

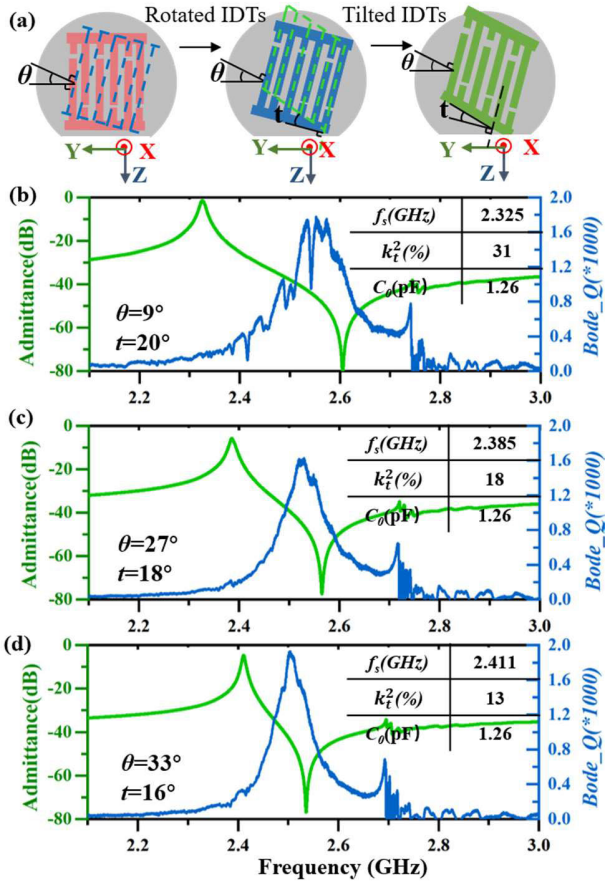

Fig. 10. (a) IDT structure schematic of the fabricated resonators. Measured admittance and *Bode_Q* curves with different in-plane orientations (b) $\theta = 9°$, (c) $\theta = 27°$, and (d) $\theta = 33°$.

Following electron-beam lithography and lift-off processes, we fabricate the eight filters in-house. These devices are measured with a 50 Ω terminal impedance utilizing the vector network analyzer in the air. Fig. 11 demonstrates the measured S-parameter responses of the filters together with their corresponding optical image. The implemented filters exhibit good passband characteristics, and feature out-of-band of rejection more than 35 dB. The critical characteristics of the filters are outlined in Table II. The center frequency and bandwidth of the filters deviated slightly from the target bands due to preparation deviations. By presetting the in-plane orientations

TABLE I
KEY DESIGN PARAMETERS OF RESONATORS IN THE EIGHT FILTERS

	θ (°)	λ (μm)	C_0 (pF)	θ (°)	λ (μm)	C_0 (pF)
	n66 Tx (Metal duty ratio 0.5)			**n25 Tx (Metal duty ratio 0.5)**		
S_1/S_3	**37.5**	2.277	1.38	**39**	2.08	1.28
S_2	**37.5**	2.269	0.57	**39**	2.074	0.53
P_1/P_2	**37.5**	2.391	4.56	**39**	2.173	4.23
	n25 Rx (Metal duty ratio 0.5)			**n66 Rx (Metal duty ratio 0.5)**		
S_1/S_3	**39**	1.981	1.28	**37.5**	1.778	1.17
S_2	**39**	1.974	0.53	**37.5**	1.772	0.48
P_1/P_2	**39**	2.063	3.88	**37.5**	1.864	3.53
	n40 (Metal duty ratio 0.5)			**2.4G Wi-Fi (Metal duty ratio 0.5)**		
S_1/S_3	**36**	1.586	0.76	**36**	1.511	0.7
S_2	**36**	1.583	0.37	**36**	1.508	0.37
P_1/P_2	**36**	1.674	3.6	**36**	1.597	3.63
	n41 (Metal duty ratio 0.3)			**n78 (Metal duty ratio 0.5)**		
S_1/S_3	**27**	1.473	1.32	**10**	0.94	0.72
S_2/S_4	**27**	1.458	0.42	**10**	0.93	0.3
P_1/P_3	**27**	1.586	2.65	**10**	1.09	1.9
P_2	**27**	1.576	2.79	**10**	1.08	2

TABLE II
CRITICAL CHARACTERISTICS OF THE FABRICATED FILTERS

Filter	n66 Tx	n25 Tx	n25 Rx	n66 Rx	n40	Wi-Fi	n41	n78
f_c (GHz)	1.75	1.89	1.975	2.111	2.352	2.424	2.6	3.64
IL_{min} (dB)	0.98	1.44	1.03	1.03	1.18	0.87	1.38	1.8
3dB FBW (%)	**4.2**	**3.7**	**3.7**	**4.6**	**4.1**	**4**	**7.7**	**12.4**
Preset k_t^2(%) of resonators	10	8	8	10	11	11	18	31

of resonators to obtain the desired k_t^2, low loss filters with FBW varied from 3.7% to 12.4% and insertion losses (ILs) less than 2 dB are demonstrated, showing the great multiband integration capability of the X-cut LNOSiC material platform.

B. High Steepness Filter Design and Fabrication

As the n41 operating frequency regime is close to the active 2.4 GHz Wi-Fi spectrum, the need for a filter with high steepness to meet the strict isolating requirements is obvious [40]. Therefore, the steepness of the n41 filter at the lower passband edge needs to be further optimized. Fig. 12 shows the simulated S-parameter responses of four seven-order ladder-type n41 filters. The MBVD model is employed to simulate the frequency response of these resonators, and then the MBVD models of corresponding resonators are connected according to a ladder-type circuit network to simulate the filter response. In the case of Filter #1, the k_t^2 of all built-in resonators is 18%, which shows good out-of-band rejection. The rejection of this filter increases from 5 to 30 dB within 26 MHz, which does not satisfy the steepness requirement of the n41 filter in rejection within the 2.4 GHz Wi-Fi band. Filter #2 employs a simultaneous reduction k_t^2 of all resonators to 16%, which results in a slight improvement in steepness. The low-frequency side

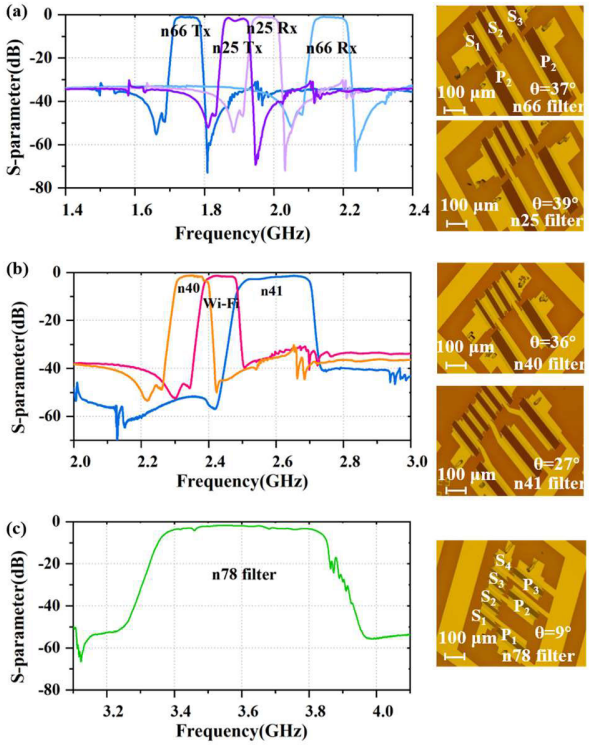

Fig. 11. Measured S-parameter responses of filters together with their optic images (a) n66 and n25 filters and (b) n40, Wi-Fi, and n41 filters, and (c) n78 filter.

rejection increases from 5 to 30 dB within 19 MHz. On the other hand, the Filter #3 only reduces the k_t^2 of resonator P_2 to 13%, and achieves the same steepness as that of Filter #2, while the out-of-band rejection of Filter #3 is significantly better. Filter #4 further reduces the k_t^2 of resonator P_2 to 7%, a further increase in skirt steepness can be achieved, and the rejection increases from 5 to 30 dB within 12 MHz. The simulation results demonstrate that selectively reducing the k_t^2 for some resonators in the topology can improve the skirt steepness of the n41 filter significantly. The proposed method holds significant advantages over the early filter design strategy that synchronous reduction of the k_t^2 of all resonators.

Based on the four filter design schemes mentioned above, four n41 filters based on the X-cut LNOSiC substrate are fabricated. Table III shows the key design parameters of resonators in the four n41 bandpass filters. Fig. 13 demonstrates the measured S-parameter responses of the filters and the corresponding admittance curves of shunt resonators. In the case of Filter #1, the in-plane orientation θ of all resonators is 27° and the corresponding k_t^2 is about 18% the rejection increases from 5 to 25 dB within 31 MHz. For Filter #2, the k_t^2 of all resonators are reduced to 16% by altering their in-plane orientation to 29°, supporting a rejection increase from 5 to 25 dB within 28 MHz. For Filter #3, the same steepness as that of Filter #2 is achieved by merely altering the in-plane orientation of resonator P_2 to 32°. For Filter #4, the k_t^2 of resonator P_2 is reduced to 7% by altering the in-plane orientation to 39°, a 5 to 25 dB rejection increase within the 16 MHz frequency range is obtained. The resonator P_2 plays a key role in the steepness of the band side. The rest

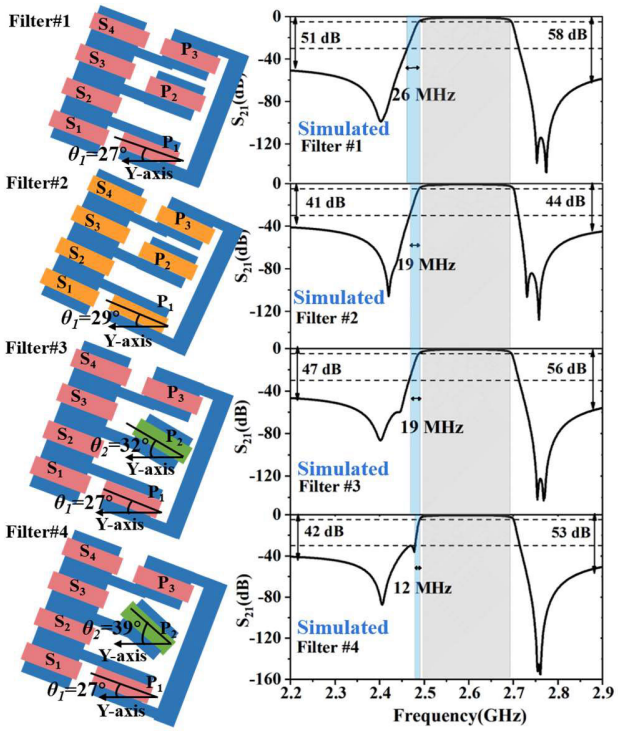

Fig. 12. Simulated S-parameter responses of four n41 bandpass filters and the corresponding structure schematics. (In the case of Filter #1, the k_t^2 of all the resonators is 18%, For the Filter #2, the k_t^2 of all the resonators is 16%. For the Filter #3, only the k_t^2 of one of shunt resonators is 13%, and all the others is 18%. For the Filter #4, only the k_t^2 of one of the shunt resonators is 7%, all the others are 18%.)

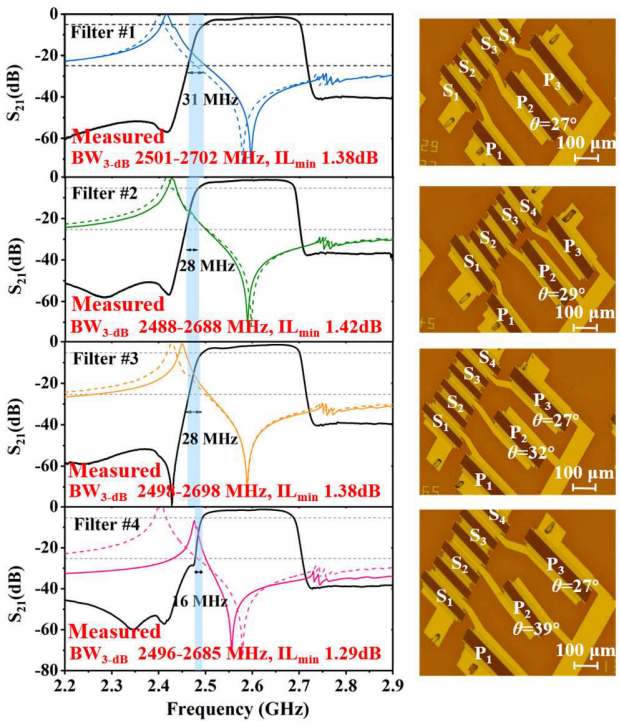

Fig. 13. Measured S-parameter responses of four band41 filters and corresponding the admittance curves of their shunt resonators, together with their optic images.

TABLE III

KEY DESIGN PARAMETERS OF RESONATORS IN THE FOUR N41 BANDPASS FILTERS

	θ (°)	λ (μm)	C_0 (pF)	θ (°)	λ (μm)	C_0 (pF)
	Filter #1 (Metal duty ratio 0.3)			**Filter #2 (Metal duty ratio 0.3)**		
S_1/S_3	**27**	1.473	1.32	**29**	1.478	2.17
S_2/S_4	**27**	1.458	0.42	**29**	1.460	0.52
P_1/P_3	**27**	1.586	2.65	**29**	1.580	2.32
P_2	**39**	1.576	2.79	**29**	1.567	2.43
	Filter #3 (Metal duty ratio 0.3)			**Filter #4 (Metal duty ratio 0.3)**		
S_1/S_3	**27**	1.473	1.31	**27**	1.471	1.28
S_2/S_4	**27**	1.462	0.45	**27**	1.467	0.51
P_1/P_3	**27**	1.586	2.65	**27**	1.586	2.65
P_2	**32**	1.565	2.1	**39**	1.561	1.4

TABLE IV

KEY DESIGN PARAMETERS OF RESONATORS IN THE 2.4 GHZ WI-FI BANDPASS FILTER

2.4 GHz Wi-Fi filter				
	θ (°)	λ (μm)	C_0 (pF)	Metal duty ratio
S_1/S_3	**36**	1.588	0.74	0.3
S_2	**40**	1.662	0.51	0.3
P_1/P_2	**36**	1.591	3.7	0.3

shunt resonators are left with nominal propagating orientation, their resonant frequency is pulled in the Wi-Fi band to create notches, maintaining the rejection throughout the 2.4 GHz Wi-Fi spectrum.

The experimental results and the simulated results show some deviations, especially in the out-of-band spectrum. These discrepancies can be attributed to the parasitic electromagnetic effect of the filter layout. These effects can be mitigated by optimizing the layout design. Regardless of the discrepancies, these experimental results still demonstrate a consistent trend with the simulation results, indicating that altering the in-plane orientation of certain resonators in a ladder-type filter to decrease their k_t^2 leads to a noteworthy enhancement in filter steepness with minimal loss. This approach holds significant advantages over the traditional scheme based on equal k_t^2 resonators.

Based on the X-cut LNOSiC substrate, the 2.4 GHz Wi-Fi bandpass filter is also optimized. The key design parameters are listed in Table IV. Fig. 14(b) shows the S-parameter response and the admittance curves of its component resonators. Analogous to the situation on the low-frequency side, the steepness of high-frequency side can be tuned by selectively reducing the k_t^2 of the series resonator. Hence, to improve the skirt steepness with low loss in the passband and the high rejection in n41, the in-plane orientation of all other resonators is chosen as 36°, corresponding to a k_t^2 near 11%. Only one of the series resonators has an in-plane orientation of 40°, corresponding to a k_t^2 near 6.5% [see Fig. 14(a)]. This filter attains a rejection increasement from 5 to 30 dB within 12 MHz.

Great mutual isolation between the 2.4 GHz Wi-Fi filter and n41 Filter #4 can be accessed via our proposed method, as is shown in Fig. 14(c). The n41 Filter #4 demonstrates a 3-dB passband of 2496–2685 MHz, a minimum IL of 1.29 dB,

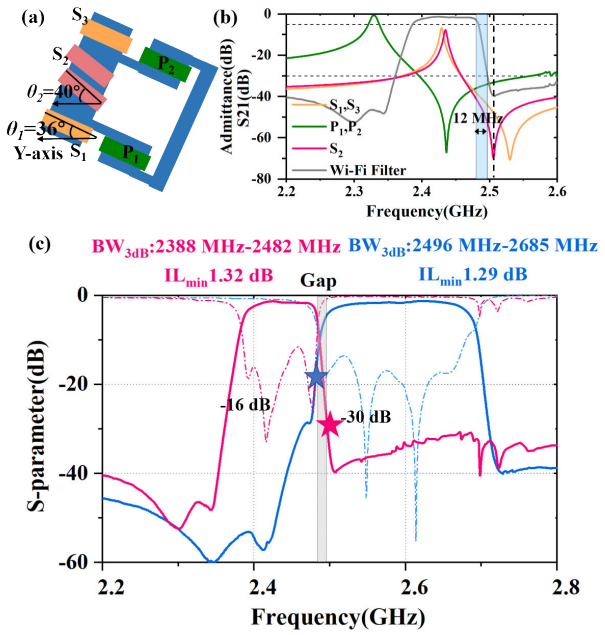

Fig. 14. (a) Structure schematic of 2.4 GHz Wi-Fi filter, (b) measured S_{21} curve of Wi-Fi filter and corresponding resonators admittance curves, and (c) measured response of 2.4 GHz Wi-Fi and n41 bandpass filters.

and reaches 16 dB rejection at 2483 MHz on the edge of the Wi-Fi band. Moreover, the typical rejection over the entire Wi-Fi band is greater than 40 dB. The 2.4 GHz Wi-Fi filter shows a 3-dB passband of 2388–2482 MHz and a minimum IL of 1.32 dB. The Wi-Fi filter achieves 30 dB rejection at 2496 MHz on the edge of the n41, the typical rejection over the entire n41 is close to 40 dB. Both filters meet the stringent coexistence requirements. Both filters adopt the method of selectively reducing the k_t^2 for some resonators in the ladder by altering the in-plane orientation. The obtained steep skirts and high rejection throughout the nearby band demonstrate the feasibility of the scheme to enhance the filter performance.

V. Conclusion

In summary, based on the X-cut LNOSiC substrate, a simple method to adjust the k_t^2 of SAW resonators within a large design window without reducing their Q values was proposed. The in-plane orientations of the resonators are adjusted to obtain the desired k_t^2. For resonators with θ from 0° to 42°, k_t^2 is continuously adjustable from 31% to 5%, while the measured maximum *Bode Q* values are maintained around 1800. By presetting the appropriate in-plane orientations of the built-in resonators, the n25, n66, n40, 2.4 GHz Wi-Fi, n41, and n78 filters with FBW from 3.7% to 12.4% and out-of-band rejection over 35 dB were demonstrated, where the n41 and Wi-Fi filters show improved skirt steepness. These results demonstrate the superior ability to modulate the k_t^2 of resonators, the FBW, and skirt steepness of filters on the X-cut LNOSiC material platform.

Acknowledgment

The authors would like to thank Hongtao Xu from the Nanofabrication Laboratory and Rongxu Bai from the National Integrated Circuit Innovation Center, Fudan University, Shanghai, China, for devices fabricated support.

References

[1] K.-y. Hashimoto et al., "Recent development of temperature compensated SAW devices," in *Proc. IEEE Int. Ultrason. Symp.*, Oct. 2011, pp. 79–86.

[2] T. Takai et al., "High-performance SAW resonator on new multilayered substrate using $LiTaO_3$ crystal," *IEEE Trans. Ultrason., Ferroelectr., Freq. Control*, vol. 64, no. 9, pp. 1382–1389, Sep. 2017.

[3] E. Butaud et al., "Innovative smart Cut piezo on insulator (POI) substrates for 5G acoustic filters," in *IEDM Tech. Dig.*, San Francisco, CA, USA, Dec. 2020, p. 34.

[4] T. Takai et al., "High-performance SAW resonator with simplified $LiTaO_3/SiO_2$ double layer structure on Si substrate," *IEEE Trans. Ultrason., Ferroelectr., Freq. Control*, vol. 66, no. 5, pp. 1006–1013, May 2019.

[5] H. Xu et al., "SAW filters on $LiNbO_3$/SiC heterostructure for 5G n77 and n78 band applications," *IEEE Trans. Ultrason., Ferroelectr., Freq. Control*, vol. 70, no. 9, pp. 1157–1169, Sep. 2023.

[6] H. Zhou et al., "Surface wave and Lamb wave acoustic devices on heterogenous substrate for 5G front-ends," in *IEDM Tech. Dig.*, San Francisco, CA, USA, Dec. 2020, pp. 17.6.1–17.6.4.

[7] T. Kimura, M. Omura, Y. Kishimoto, and K. Hashimoto, "Comparative study of acoustic wave devices using thin piezoelectric plates in the 3–5-GHz range," *IEEE Trans. Microw. Theory Techn.*, vol. 67, no. 3, pp. 915–921, Mar. 2019.

[8] J. Wu et al., "Exploring low-loss surface acoustic wave devices on heterogeneous substrates," *IEEE Trans. Ultrason., Ferroelectr., Freq. Control*, vol. 69, no. 8, pp. 2579–2584, Aug. 2022.

[9] P. Warder and A. Link, "Golden age for filter design: Innovative and proven approaches for acoustic filter, duplexer, and multiplexer design," *IEEE Microw. Mag.*, vol. 16, no. 7, pp. 60–72, Aug. 2015.

[10] S. Menendez, P. de Paco, R. Villarino, and J. Parron, "Closed-form expressions for the design of ladder-type FBAR filters," *IEEE Microw. Wireless Compon. Lett.*, vol. 16, no. 12, pp. 657–659, Dec. 2006.

[11] S. Gong and G. Piazza, "Design and analysis of Lithium–Niobate-based high electromechanical coupling RF-MEMS resonators for wideband filtering," *IEEE Trans. Microw. Theory Techn.*, vol. 61, no. 1, pp. 403–414, Jan. 2013.

[12] P. Zheng et al., "Miniaturized dual-mode SAW filters using 6-inch $LiNbO_3$-on-SiC for 5GNR and WiFi 6," in *IEDM Tech. Dig.*, San Francisco, CA, USA, Dec. 2023, pp. 1–4.

[13] Y. Wang et al., "A zero TCF band 13 SAW duplexer," in *Proc. IEEE Int. Ultrason. Symp. (IUS)*, Oct. 2015, pp. 1–4.

[14] T. Murata, M. Kadota, T. Nakao, K. Matsuda, and K.-Y. Hashimoto, "Improvement of shape factor and loss of surface acoustic wave resonator filter composed of SiO_2/high-density-electrode/$LiTaO_3$," *Jpn. J. Appl. Phys.*, vol. 48, no. 7, Jul. 2009, Art. no. 07GG05.

[15] R. Su et al., "Scaling surface acoustic wave filters on LNOI platform for 5G communication," in *IEDM Tech. Dig.*, San Francisco, CA, USA, Dec. 2022, pp. 4.2.1–4.2.4.

[16] C. Moe et al., "Highly doped AlScN 3.5 GHz XBAW resonators with 16% k2eff for 5G RF filter applications," in *Proc. IEEE Int. Ultrason. Symp. (IUS)*, Las Vegas, NV, USA, Sep. 2020, pp. 1–4.

[17] A. Volatier, G. Fattinger, F. Dumont, P. Stoyanov, and R. Aigner, "Technology enhancements for high performance BAW duplexer," in *Proc. IEEE Int. Ultrason. Symp. (IUS)*, Prague, Czech Republic, Jul. 2013, pp. 761–764.

[18] P. D. Bradley et al., "A 5 mm ×mm ×1.37 mm hermetic FBAR duplexer for PCS handsets with wafer-scale packaging," in *Proc. IEEE Ultrason. Symp.*, Munich, Germany, Jul. 2002, pp. 931–934.

[19] L. Zhang et al., "Ultra-high Q of 11000 in surface acoustic wave resonators by dispersive modulation," *IEEE Electron Device Lett.*, vol. 44, no. 5, pp. 813–816, May 2023.

[20] S. Zhang et al., "Surface acoustic wave devices using lithium niobate on silicon carbide," *IEEE Trans. Microw. Theory Techn.*, vol. 68, no. 9, pp. 3653–3666, Sep. 2020.

[21] P. Zheng et al., "Near 5-GHz longitudinal leaky surface acoustic wave devices on $LiNbO_3$/SiC substrates," *IEEE Trans. Microw. Theory Techn.*, vol. 72, no. 3, pp. 1480–1488, Mar. 2024.

[22] R. Su et al., "Wideband and low-loss surface acoustic wave filter based on 15° YX-$LiNbO_3/SiO_2$/Si structure," *IEEE Electron Device Lett.*, vol. 42, no. 3, pp. 438–441, Mar. 2021.

[23] J. Shen et al., "High-performance surface acoustic wave devices using $LiNbO_3/SiO_2/SiC$ multilayered substrates," *IEEE Trans. Microw. Theory Techn.*, vol. 69, no. 8, pp. 3693–3705, Aug. 2021.

[24] K.-J. Tseng and M.-H. Li, "Frequency and coupling factor scaling of shear horizontal SAW resonators in LNOI platform," in *Proc. Joint Conf. IEEE Int. Freq. Control Symp. Int. Symp. Appl. Ferroelectr. (IFCS-ISAF)*, Keystone, CO, USA, Jul. 2020, pp. 1–3.

[25] T.-H. Hsu, K.-J. Tseng, and M.-H. Li, "Large coupling acoustic wave resonators based on $LiNbO_3/SiO_2/Si$ functional substrate," *IEEE Electron Device Lett.*, vol. 41, no. 12, pp. 1825–1828, Dec. 2020.

[26] N. F. Naumenko, "Multilayered structures using thin plates of $LiTaO_3$ for acoustic wave resonators with high quality factor," *Ultrasonics*, vol. 31, pp. 115–122, Mar. 2018.

[27] M.-H. Li, C.-Y. Chen, R. Lu, Y. Yang, T. Wu, and S. Gong, "Temperature stability analysis of thin-film lithium niobate SH0 plate wave resonators," *J. Microelectromech. Syst.*, vol. 28, no. 5, pp. 799–809, Oct. 2019.

[28] Y. Chen et al., "Spurious free SAW resonators on $LiNbO_3/SiO_2$/quartz substrate for wideband application," in *Proc. Joint Conf. Eur. Freq. Time Forum IEEE Int. Freq. Control Symp. (EFTF/IFCS)*, May 2023, pp. 1–4.

[29] D. Psychogiou, R. Gómez-García, and D. Peroulis, "High-Q bandpass filters using hybrid acoustic-wave-lumped-element resonators (AWLRs) for UHF applications," in *IEEE MTT-S Int. Microw. Symp. Dig.*, Phoenix, AZ, USA, May 2015, pp. 1–4.

[30] C. Zuo, C. He, W. Cheng, and Z. Wang, "Hybrid filter design for 5G using IPD and acoustic technologies," in *Proc. IEEE Int. Ultrason. Symp. (IUS)*, Oct. 2019, pp. 269–272.

[31] N. F. Naumenko, "High-velocity non-attenuated acoustic waves in $LiTaO_3$/quartz layered substrates for high frequency resonators," *Ultrasonics*, vol. 95, pp. 1–5, May 2019.

[32] M. Kadota, T. Ogami, T. Kimura, and K. Daimon, "Tunable filters using wideband elastic resonators," *IEEE Trans. Ultrason., Ferroelectr., Freq. Control*, vol. 60, no. 10, pp. 2129–2136, Oct. 2013.

[33] S. Amari and G. Macchiarella, "Synthesis of inline filters with arbitrarily placed attenuation poles by using nonresonating nodes," *IEEE Trans. Microw. Theory Techn.*, vol. 53, no. 10, pp. 3075–3081, Oct. 2005.

[34] A. Giménez, J. Verdú, and P. De Paco Sánchez, "General synthesis methodology for the design of acoustic wave ladder filters and duplexers," *IEEE Access*, vol. 6, pp. 47969–47979, 2018.

[35] S. Wu et al., "Tilted IDT designs for spurious modes suppression in $LiNbO_3/SiO_2/Si$ SAW resonators," *IEEE Trans. Electron Devices*, vol. 70, no. 11, pp. 5831–5838, Nov. 2023.

[36] H. Iwamoto, T. Takai, Y. Takamine, T. Nakao, T. Fuyutsume, and M. Koshino, "Transverse modes in I.H.P. SAW resonator and their suppression method," in *Proc. IEEE Int. Ultrason. Symp. (IUS)*, Oct. 2018, pp. 1–4.

[37] J. Wu et al., "Quality factor degradation due to the in-plane misorientation in POI-SAW resonators," in *Proc. IEEE Int. Ultrason. Symp. (IUS)*, Venice, Italy, Oct. 2022, pp. 1–4.

[38] H. Yao et al., "Enhancement of quality factor using dummy electrodes at nonsymmetric in-plane rotation angles in $LiTaO_3/SiO_2$/sapphire SAW resonators," in *Proc. IEEE Int. Ultrason. Symp. (IUS)*, Montreal, QC, Canada, Sep. 2023, pp. 1–3.

[39] E. Butaud et al., "Smart Cut piezo on insulator (POI) substrates for high performances SAW components," in *Proc. IEEE Int. Ultrason. Symp. (IUS)*, Las Vegas, NV, USA, Sep. 2020, pp. 1–4.

[40] S. Kreuzer, A. Volatier, G. Fattinger, and F. Dumont, "Full band 41 filter with high Wi-Fi rejection–design and manufacturing challenges," in *Proc. IEEE Int. Ultrason. Symp. (IUS)*, Taipei, Taiwan, Oct. 2015, pp. 1–4.

Xiaoli Fang (Student Member, IEEE) received the B.E. degree in microelectronics science and engineering from Jiangnan University, Wuxi, China, in 2021. She is currently pursuing the Ph.D. degree at Shanghai Institute of Microsystem and Information Technology, Chinese Academy of Sciences, Beijing, China.

Her current research interests involve the simulation and design of surface acoustic wave (SAW) devices, including resonators, sensors, and filters.

Jinbo Wu (Member, IEEE) received the Ph.D. degree in microelectronics and solid-state electronics from Shanghai Institute of Microsystem and Information Technology, Chinese Academy of Sciences, Beijing, China, in 2023.

His current research interests include SAW/BAW/Plate wave resonators, filters, and sensors.

Shibin Zhang (Member, IEEE) received the B.E. degree from Southeast University, Nanjing, China, in 2015, and the Ph.D. degree from the University of Chinese Academy of Sciences, Beijing, China, in 2020.

He is currently a Professor at Shanghai Institute of Microsystem and Information Technology, Chinese Academy of Sciences. His current research interests include piezoelectric micro-devices on heterogeneous substrates.

Dr. Zhang received the 2022 Microwave Prize from the IEEE Microwave Theory and Techniques Society.

Pengcheng Zheng (Graduate Student Member, IEEE) received the B.E. degree in electronic science and technology from Southeast University, Nanjing, China, in 2019. He is currently pursuing the Ph.D. degree at Shanghai Institute of Microsystem and Information Technology, Chinese Academy of Sciences, Beijing, China.

His current research interests include microwave filter synthesis, the design of surface acoustic waves (SAW), and lamb wave devices.

Juxing He (Student Member, IEEE) received the B.E. degree in physics of materials from Nankai University, Tianjin, China, in 2020, and the M.E. degree in materials and chemical engineering from the National Center of Nano Science and Technology, Chinese Academy of Sciences, Beijing, China, in 2023. He is currently pursuing the Ph.D. degree at Shanghai Institute of Microsystem and Information Technology, Chinese Academy of Sciences.

His current research interests include novel micro-acoustic devices, acoustic metamaterials, and interdisciplinary applications of micro-acoustic devices.

Xinjian Ke (Student Member, IEEE) received the B.E. degree in electronic science and technology from Dalian University of Technology, Dalian, China, in 2020. He is currently pursuing the Ph.D. degree in microelectronics and solid-state electronics at Chinese Academy of Sciences, Shanghai, China.

He joined the State Key Laboratory of Materials for Integrated Circuits, Shanghai Institute of Microsystem and Information Technology, Chinese Academy of Sciences. His research interests include the research and development of piezoelectric hybrid substrates meanwhile the design of surface acoustic wave devices.

Kai Huang received the B.E. degree in microelectronics from Jilin University, Changchun, China, in 2013, and the Ph.D. degree in microelectronics and solid-state electronics from Chinese Academy of Sciences (CAS), Beijing, China, in 2018.

He is currently an Associate Professor at Shanghai Institute of Microsystem and Information Technology, CAS. His current research interests include the research and development and mass production of piezo thin films on heterogeneous substrates.

Jicong Zhao (Member, IEEE) received the Ph.D. degree in microelectronics and solid-state electronics from the Institute of Semiconductors, Chinese Academy of Sciences, Beijing, China, in 2017.

He is currently an Associate Professor at the School of Microelectronics and School of Integrated Circuits, Nantong University, Nantong, China. His research interests include RF MEMS resonators and filters and microsystem integration.

Haiyan Sun received the Ph.D. degree in electronic science and technology from Southeast University, Nanjing, China, in 2014.

He is currently an Associate Professor at the School of Microelectronics and School of Integrated Circuits, Nantong University, Nantong, China. His current research interests include the architecture, design, and simulation solutions for 2.5-D and 3-D ICs.

Min Zhou received the bachelor's degree from Donghua University, Shanghai, China, in 2017.

He is currently a Senior Engineer at Shanghai Institute of Microsystems and Information Technology, CAS, Shanghai. He is responsible for the operation and maintenance of the entire laboratory platform, specializing in ion implantation technology in the "universal ion knife" technology.

Xiaomeng Zhao received the Ph.D. degree in III-V lasers and detector material preparation from the Institute of Semiconductor, Chinese Academy of Sciences, Beijing, China, in 2017.

From 2017 to 2018, he was the head of the technical epitaxial department at Advanced Compound Semiconductors Company Ltd., Xiamen, China, and was responsible for the 6-in VCSEL laser project. Currently, he is a post-doctoral and Senior Engineer at Shanghai Institute of Microsystem and Information Technology, Chinese Academy of Sciences. His current research interests include silicon-based piezoelectric single-crystal thin film materials and silicon-based hybrid integration technology development. He has authored more than ten related papers and has been authorized more than 40 patents.

Xin Ou (Senior Member, IEEE) received the Ph.D. degree in microelectronics and solid-state electronics from Shanghai Institute of Microsystem and Information Technology (SIMIT), Chinese Academy of Sciences, Shanghai, China, in 2010.

He is currently a Professor and the Director of the Laboratory of Silicon-based Materials and Integrated Devices, SIMIT. He has authored more than 200 SCI/EI papers and has been authorized 100 patents. His current research interests include the hetero-integration of functional materials for high-performance electrical, optical, and acoustical devices, especially the piezoelectric hybrid substrate for 5G RF-filter application.

Dr. Ou was a recipient of the 2022 Microwave Prize granted by IEEE Microwave Theory and Technology Society (MTT-S), the IBMM Prize granted by the 20th International Conference on Ion Beam Modification of Materials, the Young Investigator Award granted by the 18th International Conference on Ion Implantation Technology (IIT) in 2010, the Research Prize of Helmholtz Zentrum Dresden Rossendorf Germany, the Beijing Science and Technology Progress Award (first grade), the 2019 Ten Achievements of Optics in China, and the Excellent Doctor Degree Dissertation Award of the Chinese Academy of Sciences.